JOURNAL OF CATALYSIS 132, 498–511 (1991)

FT-IR and Solid-State NMR Investigation of Phosphorus Promoted Hydrotreating Catalyst Precursors

ELAINE C. DECANIO,*,†,[1] JOHN C. EDWARDS,* THOMAS R. SCALZO,* DAVID A. STORM,* AND JOSEPH W. BRUNO†

*Texaco Inc., P.O. Box 509, Beacon, New York 12508; and †Wesleyan University, Middletown, Connecticut 06459

Received June 18, 1991; revised August 9, 1991

The effect of phosphorus on the structure of Ni–Mo/Al_2O_3 hydrotreating catalyst precursors has been investigated. Calcined and reduced P/Al_2O_3, P–Ni/Al_2O_3, P–Mo/Al_2O_3, and P–Ni–Mo/Al_2O_3 (where the wt% P = 0.0 to 10.0, wt% Mo = 8.0 to 12.0, and wt% Ni = 4.0) have been studied using FT-IR, XRD, and ^{31}P and ^{27}Al MAS NMR techniques. Phosphoric acid reacts with alumina hydroxyls forming monomeric and polymeric phosphates. At the higher phosphorus loadings, aluminum phosphate is also formed. On calcined P–Ni/Al_2O_3, nickel phosphate is formed. This leads to a decrease in density of Ni^0 sites in the reduced state as measured by CO adsorption. The addition of up to 1.5 wt% P to Mo(8)/Al_2O_3 promotes the formation of octahedral molybdena on the alumina surface. However, the addition of >2.0 wt% P results in the formation of bulk MoO_3 and $Al_2(MoO_4)_3$ in both P–Mo(8)/Al_2O_3 and P–Mo(12)/Al_2O_3. CO adsorption on reduced P–Ni(4)–Mo(8)/Al_2O_3 samples shows that the presence of 0.5 wt% P causes a significant increase in the number of sites adsorbing CO. Increasing the P loading further causes a decrease in the number of adsorbing sites; this decrease can be attributed to the formation of either nickel phosphate or nickel molybdate. © 1991 Academic Press, Inc.

INTRODUCTION

New environmental regulations concerning vehicle emissions in the United States and the prospect of future crude supplies having a higher proportion of heavy fuel oil are making it necessary to develop improved hydroprocessing catalysts (*1, 2*). Toward this end, researchers are trying to identify additives which improve the activities of molybdenum based catalysts. In particular, phosphorus additives (in the form of phosphates) have stimulated a considerable amount of research (*3–14*). The presence of small amounts of phosphorus in sulfided Ni–Mo/Al_2O_3 catalysts has been shown to have a positive effect on both their HDN and HDS activities (*14–17*). In addition, phosphorus containing catalysts are less susceptible to coking (*14*). However, the surface chemistry and role of phosphorus in these systems is not well understood.

In order to understand better the role of phosphorus, we have prepared several series of catalysts (P/Al_2O_3, P–Mo/Al_2O_3, P–Ni/Al_2O_3, and P–Ni–Mo/Al_2O_3) by sequential incipient wetness impregnations, in which we varied the phosphorus loading from 0.0 to 10.0 wt%, the molybdenum loading from 8.0 to 12.0 wt%, and maintained the nickel loading at 4 wt%. In this paper we report the results of an FT-IR, XRD, and solid-state ^{31}P and ^{27}Al MAS NMR study of these catalysts in their reduced and calcined states. To our knowledge this is the first study in which both FT-IR and NMR have been used to investigate the role of phosphorus in these systems. Furthermore, it is the first study in which the one and two component systems have been analyzed in detail, and in which

[1] To whom correspondence should be addressed.

0021-9517/91 $3.00
Copyright © 1991 by Academic Press, Inc.
All rights of reproduction in any form reserved.

an attempt has been made to relate these effects to the change in the density of adsorption sites on the reduced P–Ni–Mo/Al_2O_3 system as the phosphorus loading is changed.

EXPERIMENTAL

Sample Preparation

All samples were prepared by the aqueous incipient wetness impregnation technique. Norton 6375C Gamma Alumina (20/40 mesh) was used as the support. It has a surface area of 221.8 m^2/g and a pore volume of 1.4 cc/g. Phosphoric acid, ammonium heptamolybdate ($(NH_4)_6Mo_7O_{24} \cdot 4H_2O$), and nickel nitrate ($NiNO_3 \cdot 6H_2O$) were used as the starting materials. P/Al_2O_3 samples were prepared and dried at 393 K for 16 h. The P–Mo/Al_2O_3 and P–Ni/Al_2O_3 were prepared by impregnating dried P/Al_2O_3 with appropriate solutions of either nickel or molybdenum. These samples were dried at 373 K for 16 h and then calcined in flowing air (60 cc/min) at 773 K for 3 h. P–Ni–Mo/Al_2O_3 samples were prepared by impregnating calcined P–Mo/Al_2O_3 with nickel solutions, followed by drying and calcining.

The metal loadings of every sample were confirmed by elemental analysis.

Infrared Studies

IR spectra were collected using a Nicolet 170 sx FT-IR spectrometer with a liquid nitrogen cooled MCT detector. All spectra were recorded after 100 scans with a resolution of 4 cm^{-1}. Spectra were measured using a quartz cell with NaCl windows attached to a glass gas handling/vacuum system. Hydrogen (ultra high purity), carbon dioxide, and carbon monoxide (99% pure), were passed through molecular sieve traps prior to use, and CO_2 was further purified by the freeze–thaw method. Self-supporting wafers, 1.6 cm in diameter, were prepared by pressing 20 mg of 325 mesh powder at 6000 psi. The wafers were mounted in the cell, evacuated for 12 h (10^{-5} Torr), and reduced at 673 K in flowing hydrogen (14 cc/min) for 1 h. The reduced samples were evacuated at 673 K for 0.5 h, and then cooled to room temperature. For CO_2 adsorption, the sample was exposed to 50 Torr CO_2 for 0.5 h, followed by evacuation. For CO adsorption, the samples were exposed to 100 Torr of 0.5 h, followed by evacuation to 20 Torr for 0.5 h, then a final evacuation to 10^{-5} for 0.5 h.

NMR Studies

The solid-state ^{27}Al and ^{31}P NMR spectra were recorded on a Varian VXR-300 FT-NMR equipped with a Chemagnetics solids accessory, operating at resonance frequencies of 78.3 and 121.7 MHz, respectively. The ^{31}P chemical shifts were reported relative to an 85% H_3PO_4 solution, while the ^{27}Al shifts are relative to $KAl(SO_4)_2$. Both Bloch decay magic angle spinning (MAS) and cross polarization MAS experiments were performed. Typical contact times in the ^{27}Al experiments were in the range 0.2–0.5 ms, and for the ^{31}P experiments, a contact time of 2 ms was used. Spinning frequencies of 6–7 KHz were employed.

XRD Studies

The X-ray diffraction patterns were collected using a Scintag, PAD IV, theta/2 theta diffractometer. The diffractometer is equipped with a 2-degree divergence slit, a 0.3-mm receiving slit, and an intrinsic germanium solid state detector. The samples were ground to a 100-mesh particle size, and top loaded into the cell. The run conditions used are as follows: power, 45 kV 40 mA; source, Cu K-alpha; range: 5°–70° 2-theta at 0.03 step size at a continuous rate of 0.5° per min.

RESULTS AND DISCUSSION

P/Al_2O_3

The IR spectra of the hydroxyl region of reduced P/Al_2O_3 samples (wt% P = 0.0, 0.5, 1.5, 2.0, 4.0, and 6.0) are shown in Fig. 1. The spectrum of P(0)/Al_2O_3 (where (0) denotes a zero wt% P loading) is typical of a partially dehydroxylated alumina surface

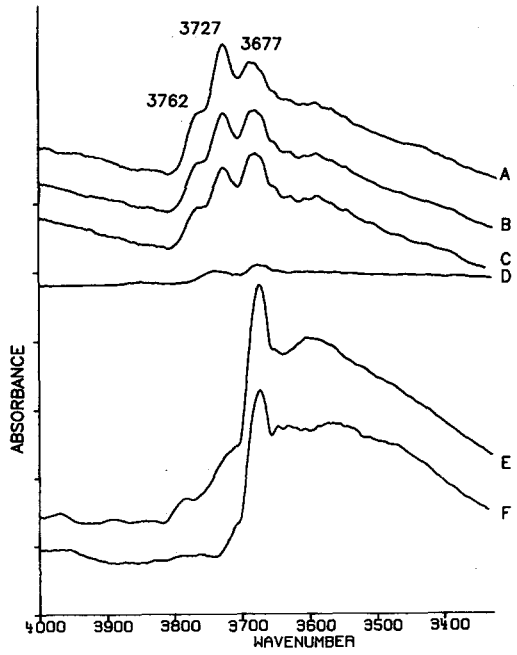

FIG. 1. IR spectra of the hydroxyl region of reduced P/Al_2O_3: (A), 0.0 wt% P; (B), 0.5 wt% P; (C), 1.5 wt% P; (D), 2.0 wt% P; (E), 4.0 wt% P; (F), 6.0 wt% P.

with IR bands at 3677, 3727, and 3762 cm^{-1}. The positions of the hydroxyl bands have been shown to be dependent on the acidity of the hydroxyl group; the most basic hydroxyl groups give rise to the IR bands between 3760 and 3778 cm^{-1}, while the most acidic hydroxyl groups produce bands at 3740 cm^{-1} (*18, 19*). Therefore, the 3762 cm^{-1} band, observed for $P(0)/Al_2O_3$, is assigned to the more basic hydroxyl groups and the 3677 cm^{-1} band is due to the more acidic hydroxyl groups. The IR data reveal that for phosphorus loadings up to 1 wt%, the phosphoric acid reacts with the basic hydroxyl groups as evidenced by the loss of intensity of the 3762 cm^{-1} band. Then, between 1 and 2 wt% phosphorus, there is a dramatic decrease in the intensity of all the hydroxyl bands, showing that at higher phosphorus loadings phosphoric acid reacts with all the hydroxyl groups. At 4 and 6 wt% P, no alumina hydroxyl bands are apparent, but there is a band at 3670 cm^{-1} which is due to the OH associated with the phosphate (*20*). The broad band at 3558 cm^{-1}, observed for $P(4)/Al_2O_3$, can be assigned to strongly held water.

CO_2 adsorption confirmed that the addition of phosphorus results in the depletion of surface hydroxyl groups (Fig. 2). The IR spectrum of CO_2 adsorbed on Al_2O_3 produces bands at 1232, 1451, 1475, and 1646 cm^{-1}, which are due to the asymmetric OCO stretch of the HCO_3^-, the symmetric OCO stretch of the CO_3^{2-}, the symmetric stretch of the HCO_3^-, and the C–OH bend of the HCO_3^-, respectively (*21*). The HCO_3^- is formed by the reaction between CO_2 and the alumina hydroxyl groups (*21*). CO_2 chemisorption has been used previously to monitor the density of surface hydroxyl groups on Mo/Al_2O_3 catalysts (*22, 23*). Increasing the phosphorus loading up to 4 wt% P results in the systematic decrease in intensity of the HCO_3^- bands. CO_2 adsorption on $P(4)/Al_2O_3$ does not produce any bands in the carbonate region; this confirms that the hydroxyl group associated with the phosphorus is acidic in nature.

These results show that phosphoric acid initially reacts with the most basic alumina hydroxyls, and then, as the phosphorus loading is increased, it reacts with the acidic hydroxyls also. This is in agreement with the results of other workers (*6*). However, even though it is generally believed that the reaction between phosphoric acid and the alumina hydroxyls produces surface phosphates (*4, 6, 12, 13*), the exact nature of the phosphate species has not been fully determined.

X-ray diffraction patterns of dried P/Al_2O_3 samples were collected (spectra not shown). Assignment of the diffraction patterns was achieved by comparing our data with those in the library of diffraction patterns supplied with the software. Increasing the phosphorus loading causes a small, but systematic decrease in the intensity of the diffraction peaks due to the aluminum oxide at 2-theta = 67°, 46°, 39.5°, and 37.5°, indicating that the alumina surface is being cov-

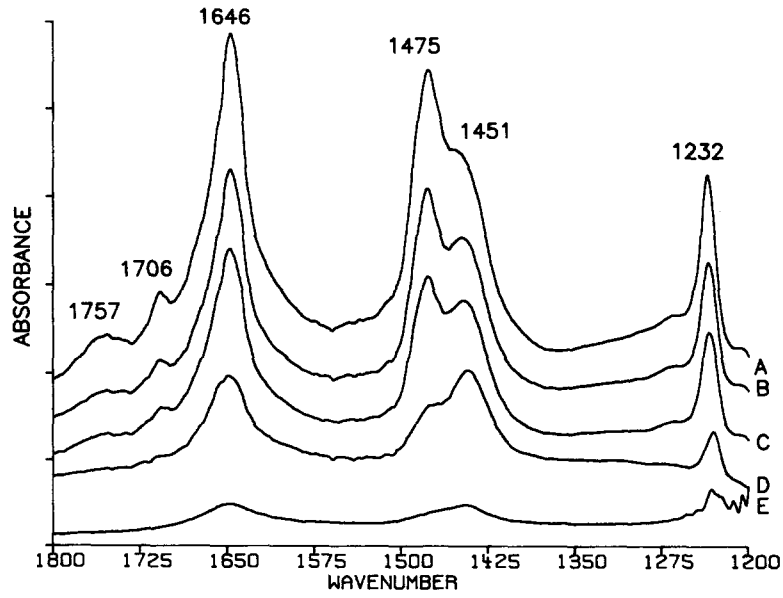

FIG. 2. IR spectra of CO_2 adsorbed on reduced P/Al_2O_3 samples: (A), 0.0 wt% P; (B), 0.5 wt% P; (C), 1.5 wt% P; (D), 2.0 wt% P; (E), 4.0 wt% P.

ered by an amorphous species which is not detected by XRD. No peaks due to bulk aluminum phosphate are observed until 9 wt% P is present. Increasing the phosphorus loading above 9 wt% results in a progressive increase in diffraction peaks at 2-theta = 21° and 20° due to bulk aluminum phosphate. The formation of aluminum phosphate is not unexpected since it has been shown that upon impregnation of the phosphoric acid, partial solubilization of the Al^{3+} ion occurs and $AlPO_4$ is precipitated during the drying procedure. The effect of sample pretreatment was also investigated using XRD. Calcination or hydrogen reduction of $P(6)/Al_2O_3$ causes a loss of intensity of the aluminum phosphate diffraction peaks, revealing that these treatments cause the aluminum phosphate crystallites to disperse into amorphous aluminum phosphate (*5*).

In order to characterize more fully the phosphate species present on the alumina surface, we have carried out ^{31}P and ^{27}Al Bloch decay (BD) and cross polarization (CP) MAS NMR experiments. The ^{31}P BD/MAS of dried $P(x)/Al_2O_3$ (where the P loading is varied from 1.0 to 10.0 wt%) is shown in Fig. 3. $P(1)/Al_2O_3$ produces a resonance at -10 ppm. Increasing the phosphorus loading causes a systematic upfield shift of this resonance so that at $P(4)/Al_2O_3$ the resonance is at -20 ppm. At 5 wt% P, the resonance is centered at -20 ppm, but a shoulder appears near -26 ppm. As the phosphorus loading is increased to 9 wt%, the resonance appears to have shifted still further upfield. Finally, at 10 wt% P, the signal at -32 ppm exhibits a significant gain in intensity as compared to the -20 ppm signal.

Callis and co-workers have studied the ^{31}P spectra of polyphosphate ions in aqueous solutions (*24, 25*). They find that monomeric (orthophosphate), terminal, and internal phosphate groups resonate at measurably different positions; specifically, terminal and internal phosphates exhibit resonances 5 to 10 and 18 to 21 ppm, respectively, upfield of resonances for monomeric H_3PO_4. Thus, the shifts observed for P/Al_2O_3 in the range -10 to -20 ppm can be attributed to the formation of polymeric phosphate

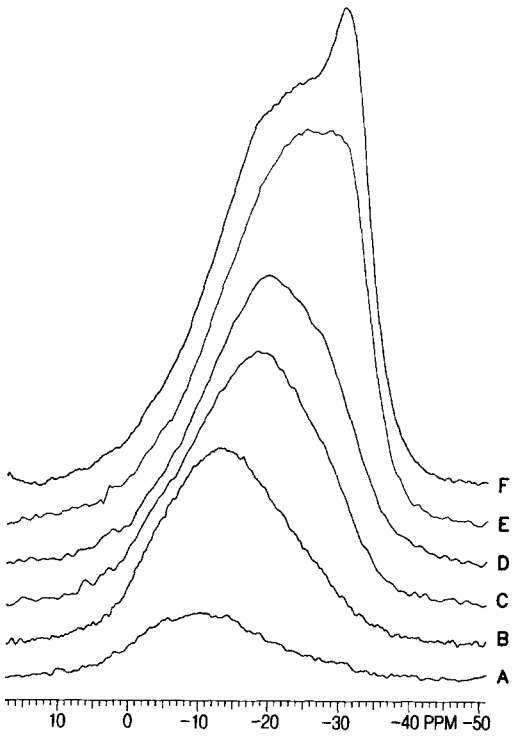

FIG. 3. ^{31}P BD/MAS NMR spectra of dried P/Al_2O_3: (A), 1.0 wt% P; (B), 3.0 wt% P; (C), 4 wt% P; (D), 5 wt% P; (E), 9 wt% P; (F), 10 wt% P.

chains. At 1 wt% P, monomeric phosphate and short chain polymeric species are condensed on the alumina surface, giving rise to the resonance at around -10 ppm. At 5 wt% P, longer polymeric phosphate chains are formed by condensation reactions. These chains contain terminal phosphate groups, resonating at about -10 ppm, and internal phosphate groups which resonate at approximately -20 ppm. Thus, at lower loading levels (0–4 wt%) the ^{31}P spectrum consists of two inhomogeneously broadened resonances from terminal and internal phosphate groups. The gradual shift from -10 to -20 ppm with increasing phosphorus loading provides a qualitative measure of the ratio of terminal to internal phosphates (*26*).

In addition to these polymeric phosphates, XRD shows that at 6 wt% P aluminum phosphate also begins to form; therefore the signal at -32 ppm could also be due, in part, to aluminum phosphate, and this is supported by the fact that crystalline $AlPO_4$ exhibits a similar chemical shift (*26*).

The CP/MAS experiment (Fig. 4) yields information on the presence of protons in the environment surrounding the phosphorus centers. The $P(1)/Al_2O_3$ CP/MAS spectrum shows a resonance at -11 ppm. There is a systematic upfield shift of this resonance with increasing phosphorus loading, so that at 10 wt% a resonance is observed at -22 ppm. It should be noted that the resonance which appears at -32 ppm in the BD/MAS spectra of the 10 wt% P sample is not observed in the CP experiment, indicating protons are not next nearest neighbors to these phosphorus species: these are phosphorus species in the crystalline $AlPO_4$.

In other investigations of pure aluminum phosphate (*27, 28*), dry $AlPO_4$ has been reported to give a resonance at -32 ppm. Hydration of the dry $AlPO_4$ is seen to cause

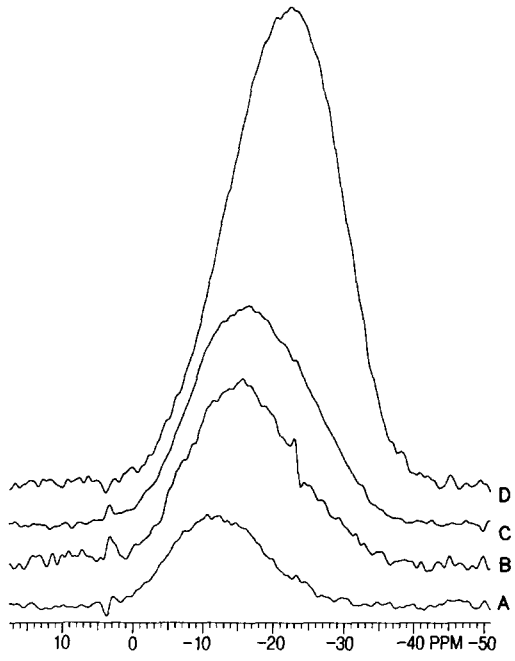

FIG. 4. ^{31}P CP/MAS NMR spectra of dried P/Al_2O_3: (A), 1.0 wt% P; (B), 3 wt% P; (C), 5.0 wt% P; (D), 10.0 wt% P.

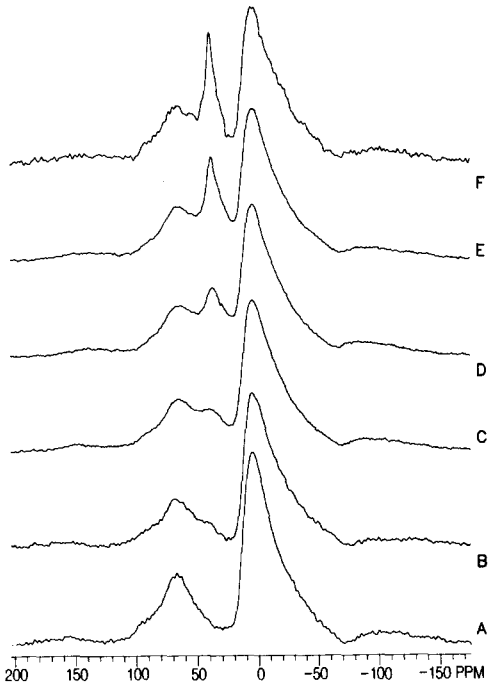

FIG. 5. ^{27}Al BD/MAS NMR spectra of dried P/Al_2O_3: (A), 0.0 wt% P; (B), 4.0 wt% P; (C), 6.0 wt% P; (D), 8.0 wt% P; (E), 9.0 wt% P; (F), 10.0 wt% P.

a splitting of this resonance into two new resonances, one at −24 ppm and the other at −32 ppm. Thus, this may provide evidence that several types of $AlPO_4$ form on the alumina surface which differ in their degrees of hydration, though these details are not readily apparent in Figs. 3 and 4.

^{27}Al BD/MAS spectra of the P/Al_2O_3 samples are shown in Fig. 5. The Al_2O_3 spectrum contains resonances at 72 ppm and 0 ppm, which can be assigned to Al^{3+} in tetrahedral and octahedral symmetries, respectively (*29*). At 4 wt% P, an additional broad signal is seen at 38 ppm which is due to amorphous aluminum phosphate. The intensity of this signal increases with phosphorus loading up to 8 wt%. At 8 wt% P another, narrower resonance appears at 40 ppm. Finally, at 10 wt% P, this narrower resonance is seen to intensify. This resonance can be attributed to crystalline aluminum phosphate (*28*).

These ^{27}Al experiments confirm the presence of aluminum phosphate on the alumina surface. In addition, our results show that this technique can also be used to differentiate between the amorphous phase, which gives rise to the rather broad resonance at 38 ppm, and the bulk crystalline phase, which gives the narrower resonance at 40 ppm. The sharpness of the resonance at 40 ppm implies that the Al^{3+} is in a very symmetrical environment in which there is very little distortion from tetrahedral symmetry. Table 1 summarizes the ^{27}Al and ^{31}P chemical shifts for the phosphate species formed on the alumina surface.

The effect of calcination on the P(10)/Al_2O_3 sample is shown in Fig. 6. The ^{27}Al BD/MAS spectra of this catalyst before, and after calcination are shown in Fig. 6(a). The signal at 40 ppm has decreased in intensity upon calcination, showing that the crystalline $AlPO_4$ is disintegrating during the calcination. This is also apparent in the ^{31}P BD/MAS spectra (Fig. 6(b)); calcination results in a decrease in intensity of the resonance at −32 ppm. The ^{31}P BD/MAS spectra also shows that there is a decrease in the density of polymeric phosphate species, as evidenced by the decrease in intensity of the resonance at −19 ppm. These results are in agreement with the XRD data, which show that calcination causes the aluminum phosphate crystals to break down to form dispersed, amorphous aluminum phosphate. These data also suggest that some polymeric phosphates are transformed into amorphous aluminum phosphate during calcination.

TABLE 1

^{27}Al and ^{31}P BD/MAS NMR Chemical Shifts for the Phosphate Species Present on the Al_2O_3 Surface

Species	^{27}Al (ppm)	^{31}P (ppm)
Monomeric phosphate	—	−10
Polymeric phosphate		
Terminal groups	—	−10
Internal groups	—	−20
Amorphous $AlPO_4$	38	−26
Crystalline $AlPO_4$	40	−32

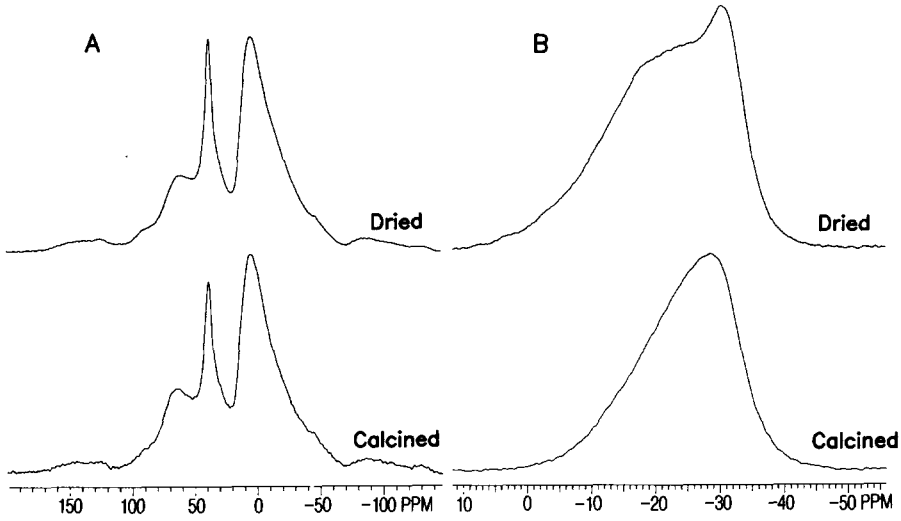

FIG. 6. NMR spectra of dried and calcined P(10)/Al_2O_3: (A) ^{27}Al BD/MAS and (B) ^{31}P BD/MAS.

We have also measured the surface areas and pore volumes of these samples (Table 2). There is a decrease in surface areas and pore volumes as the phosphorus loading is increased. Most notable is the very sudden drop in both surface area and pore volume between 6 to 10 wt% P. This large decrease can be attributed to the aluminum phosphate crystal formation which covers the alumina surface and blocks the entrance to the pores (*8*).

P–Ni/Al_2O_3

The IR spectra produced when CO is adsorbed on reduced P–Ni(4)/Al_2O are shown in Fig. 7. CO adsorption on Ni(4)/Al_2O_3 produces bands at 1950 and 2064 cm^{-1}. These bands have both been assigned to linear CO adsorbed on Ni^0: the 1950 cm^{-1} band is thought to be due to edge Ni^0 sites, while the 2064 cm^{-1} band is due to Ni^0 in the planes (*30–32*). The presence of 1.0 wt% P in the Ni(4)/Al_2O_3 sample causes a large decrease in the intensity of the 2064 cm^{-1} and the 1950 cm^{-1} bands. At progressively higher P concentrations there is a gradual decrease in intensity of both the 2064 and the 1950 cm^{-1} bands, showing that there is a decrease in surface Ni^0 as the phosphorus loading is increased.

Calcination of Ni/Al_2O_3 samples has been shown to cause some of the Ni^{2+} to enter the alumina lattice to form a nickel aluminate spinel. Several reports suggest that one of the roles of phosphorus is to increase the density of nickel species on the alumina surface by preventing the formation of nickel aluminate (*33, 34*). However, if this was the case, we would expect to observe an increase in the density of Ni^0 sites. Since our IR data reveals that this is not happening, we can conclude that it is not the role of phosphorus to prevent the formation of nickel aluminate. Nickel phosphate has

TABLE 2

Effect of Phosphorus Loading on the Surface Areas and Pore Volumes of Dried P/Al_2O_3

wt% P	Surface area (m^2g^{-1})	Pore volume (cm^3g^{-1})
0.0	221.8	1.32
0.5	207.5	1.29
3.0	189.5	1.26
5.0	184.6	1.12
6.0	182.6	1.06
8.0	144.7	0.96
10.0	135.5	0.84

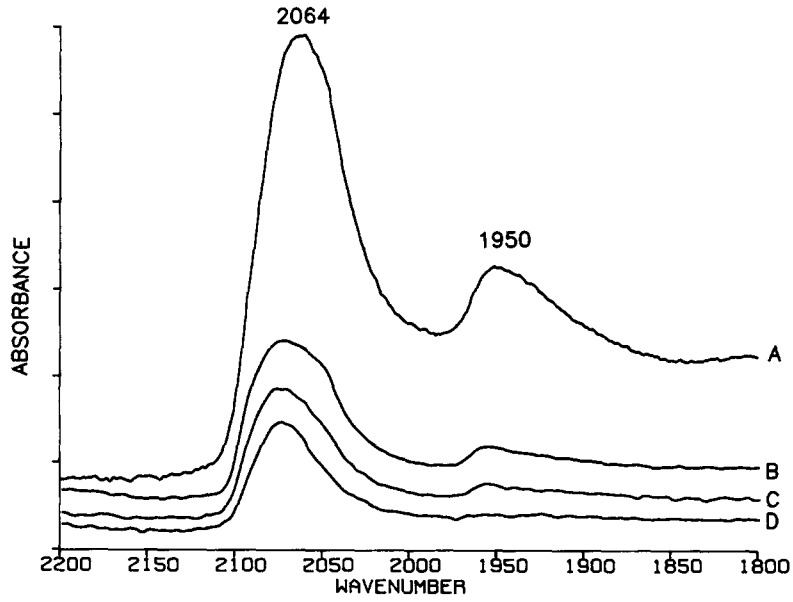

FIG. 7. IR spectra of CO adsorbed on reduced P-Ni(4)/Al_2O_3 samples: (A), 0.0 wt% P; (B), 1.0 wt% P; (C), 2.0 wt% P; (D), 3.0 wt% P.

been shown to form on carbon supported systems where there is little interaction between the phosphate and a carbon support (*35, 36*). Our IR results suggest that nickel phosphate also forms on these P–Ni/Al_2O_3 samples, as evidenced by the decrease in intensity of the Ni^0–CO band with increasing phosphorus concentration. Nickel phosphate is proposed to result from the reaction between Ni^{2+} and the anion of the polymeric phosphate during the calcination.

NMR data yielded results similar to those observed for P/Al_2O_3 catalysts. However, the presence of paramagnetic Ni^{2+} interacting with the ^{27}Al and ^{31}P species was demonstrated by the reduction of signal intensity and relaxation delays and by the baseline roll induced in the ^{31}P spectra. Reduction of intensity could also be attributed to nickel phosphate formation.

P–Mo/Al_2O_3

The IR spectra of CO adsorbed on reduced P–Mo/Al_2O_3 samples are shown in Fig. 8. CO adsorption on reduced Mo(8)/Al_2O_3 produces IR bands at 2177, 2130, 2070, and 1992 cm^{-1}. Previously, we have shown that CO adsorption can be used as a sensitive probe for the oxidation state of the molybdenum (*37*): Mo^{5+}, Mo^{4+}, physisorbed CO, and Mo^{2+} or Mo^{3+}, produce bands at 2205, 2175, 2130, and 2070 cm^{-1}, respectively. The signal at 1992 cm^{-1} is due to Mo^0 (*38–42*).

The signal at 2177 cm^{-1} (Fig. 8) is therefore due to a combination of Mo^{5+} and Mo^{4+} carbonyls. The addition of up to 1.5 wt% P causes an increase in the intensity of the 2177 cm^{-1} band, while there is no effect on the other bands. It is well known that the molybdenum oxide structures, and their reducibilities, are dependent on the molybdenum loading (*42–45*). At low molybdenum loadings, the predominant molybdenum oxide species is a monomeric, tetrahedral, MoO_4^{2-} species which is bound strongly to the alumina support and, therefore, not easily reduced. At higher molybdenum loadings, a polymeric molybdate species forms in which the molybdenum oxide has distorted octahedral symmetry and is more easily reduced. Finally, at monolayer cover-

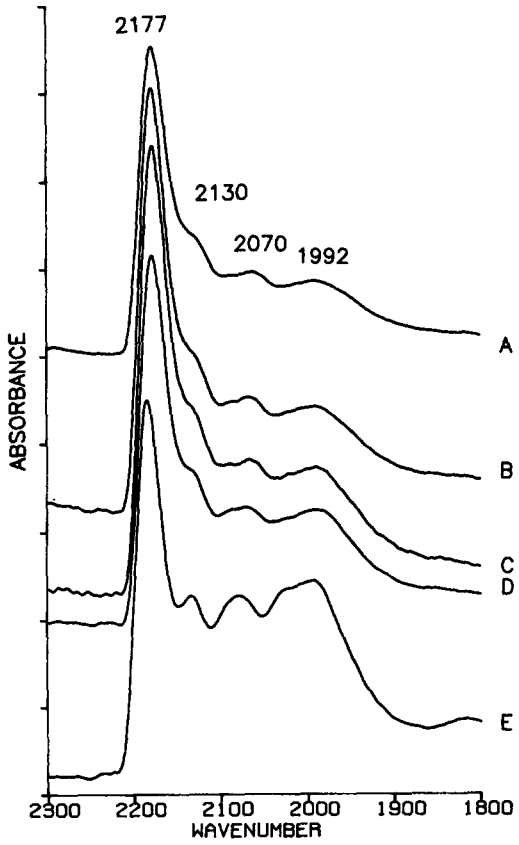

FIG. 8. IR spectra of CO adsorbed on reduced P-Mo(8)/Al_2O_3 samples: (A), 0.0 wt% P; (B), 0.5 wt% P; (C), 1.5 wt% P; (D), 2.0 wt% P; (E), 3.0 wt% P.

ages, MoO_3 and $Al_2(MoO_4)_3$ are formed; reduction of MoO_3 is very facile (*23*). The increased intensity of the 2177 cm^{-1} band therefore demonstrates that phosphates are altering the molybdenum oxide structure by promoting the formation of more octahedral molybdate species, even at low Mo loadings.

The presence of 3.0 wt% P has a large effect on the molybdenum oxide species present on the alumina surface as evidenced by changes in the IR spectrum (Fig. 8(e)). There is a systematic decrease in the intensity of the 2177 cm^{-1} band as the phosphorus loading is increased from 1.5 to 3.0 wt%. Concurrently, there is a large increase in the intensity of the band at 1992 cm^{-1}. The signal at 1992 cm^{-1} is due to Mo^0. The increase in intensity of this band, therefore, reveals that there is a greater density of Mo^0 species present on the high phosphorus reduced samples, which in turn suggests there is more bulk MoO_3 on these samples in the calcined state. At phosphorus loadings above 2 wt% the phosphate is, therefore, promoting the formation of MoO_3 at the expense of the octahedral molybdate species.

Alumina has an isoelectric point of between pH 6 and 8 and the pH of the impregnating solution has been shown to be important in determining the nature of the adsorbing molybdenum oxide species (*43–45*). In our sample preparations, the pH's of the 8 wt% Mo impregnating solutions were 6.0. Aqueous solutions of ammonium heptamolybdate are known to participate in the equilibrium shown in Eq. (1):

$$Mo_7O_{24}^{6-} + 4\,H_2O \rightleftharpoons 7\,MoO_4^{2-} + 8\,H^+. \quad (1)$$

It has been shown that for samples of low molybenum loadings prepared by the incipient wetness impregnation technique, regardless of the pH of the impregnating solution, the MoO_4^{2-} species adsorb onto the alumina surface (*44*). This is because there is a high pH at the alumina surface due to the production of hydroxide ions, as shown in Eq. (2):

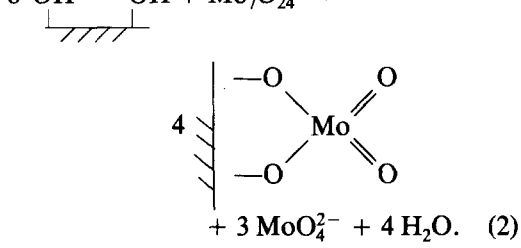

Furthermore, the adsorbing molybdenum oxide reacts with the most basic hydroxyl groups preferentially. However, at higher molybdenum concentrations, the alumina surface no longer acts as a buffer and the $Mo_7O_{24}^{6-}$ is adsorbed, either intact or as octahedral fragments.

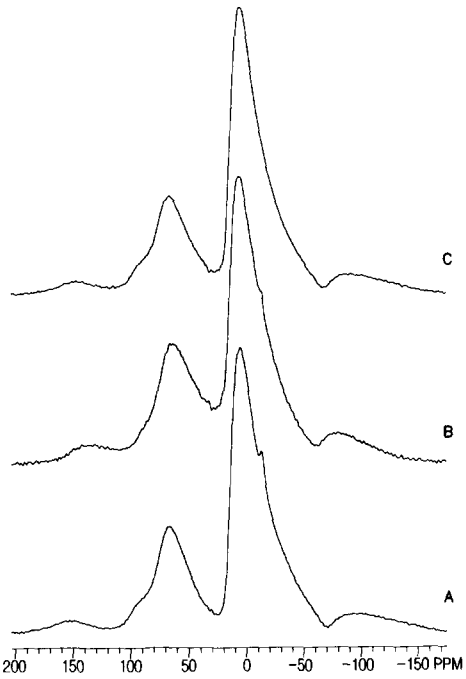

FIG. 9. ^{27}Al BD/MAS NMR spectra of calcined Mo/Al_2O_3: (A), 12.0 wt% Mo; (B), 10.0 wt% Mo; (C), 8.0 wt% Mo.

There are several reasons for which the presence of phosphates may promote the formation of octahedral molybdates at the expense of tetrahedral MoO_4^{2-}. One reason might be a competition for the basic hydroxyl groups, made more important in our samples because the phosphates have already formed prior to molybdenum impregnation. Another possibility is that the presence of phosphates alters the isoelectric point of the alumina surface, thus favoring the adsorption of the larger molybdenum oxide ions which lead to the octahedral species. Another possible explanation is that at the lower phosphate loadings the predominant phosphate species are polyphosphates, which we have shown, using ^{31}P CPMAS and FT-IR, to have hydroxyl groups which are acidic. If this is the case then the equilibrium shown in Eq. (1) would be shifted to the left, favoring the heptamolybdate species. Finally, at the higher phosphate loadings, both amorphous and crystalline aluminum phosphate species cover the alumina surface, depleting the available alumina hydroxyls so that the molybdenum oxide clusters are forced to form on the catalyst surface. Again, the acidic nature of the phosphate hydroxyl group may play a part in determining the adsorbed species.

XRD spectra of P–Mo(8)/Al_2O_3 and P–Mo(12)/Al_2O_3 confirm that the presence of phosphates promotes the formation of MoO_3 and $Al_2(MoO_4)_3$, as evidenced by the increase in the peaks at 2-theta = 23°, 25.8°, and 26.8°. However, XRD is again unable to provide a sensitive measure of the small changes that occur.

^{27}Al BD/MAS can also be used to characterize $Al_2(MoO_4)_3$ (*46*), which is formed by the reaction of MoO_3 with the alumina surface (*23*). The ^{27}Al BD/MAS spectra of calcined Mo/Al_2O_3 (wt% Mo = 8, 10, and 12) show that $Al_2(MoO_4)_3$, which resonates at −13.7 ppm, is present at molybdenum load-

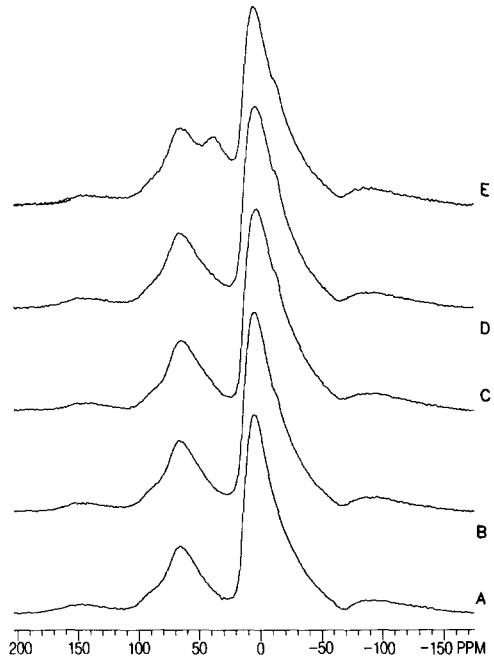

FIG. 10. ^{27}Al BD/MAS NMR spectra of calcined P-Mo(8)/Al_2O_3: (A), 0.0 wt% P; (B), 1.0 wt% P; (C), 2.0 wt% P; (D), 4.0 wt% P; (E), 6.0 wt% P.

ings of 10 wt%, and above (Fig. 9). The addition of up to 4 wt% P to Mo(8)/Al_2O_3 causes a systematic increase in the amount of $Al_2(MoO_4)_3$ present on the alumina surface, as evidenced by the increase in intensity of the resonance at −13.7 (Fig. 10); further addition of up to 6 wt% P results in the presence of amorphous aluminum phosphate (as evidenced by the appearance of the resonance at 40 ppm), and in the decrease in the amount of $Al_2(MoO_4)_3$ (as evidenced by the loss of intensity of the −13.7 ppm resonance). The decrease in the amount of $Al_2(MO_4)_3$ is probably the result of a competition between the phosphate and MoO_3 for the alumina surface.

As with the Mo(8)/Al_2O_3 samples, the addition of up to 4 wt% phosphorus to Mo(12)/Al_2O_3 causes a small increase in the $Al_2(MoO_4)_3$; this is indicated by the increase in intensity of the resonance at −13.7 ppm (Fig. 11). However, with P loadings greater than 4 wt% there is also an increase in the amount of amorphous aluminum phosphate on the alumina surface, as evidenced by the resonance at 38 ppm. The presence of a sharp signal at 40 ppm when greater than 6 wt% P is added to the Mo(12)/Al_2O_3 sample shows the presence of crystalline $AlPO_4$; this is in agreement with the XRD data. Crystalline $AlPO_4$ is formed because at a 12 wt% Mo loading there is a monolayer coverage of the alumina surface and, therefore, there is little alumina surface available for the phosphate to react with.

^{31}P BD/MAS measurements of the calcined P–Mo(8)/Al_2O_3 (Fig. 12) reveal that polymeric phosphate chains are present along with aluminum phosphate. In fact, the presence of the different resonances are more apparent for these samples than for the P/Al_2O_3 samples. In the BD/MAS spectrum of P(0.5)/Al_2O_3 there is a resonance at −17 ppm and a shoulder at approximately −8 to −10 ppm. These are due, again, to the presence of terminal and internal phosphate groups. For the samples with phosphorus loadings above 2 wt%, another signal is clearly observed at −25 ppm. This resonance is attributable to amorphous aluminum phosphate.

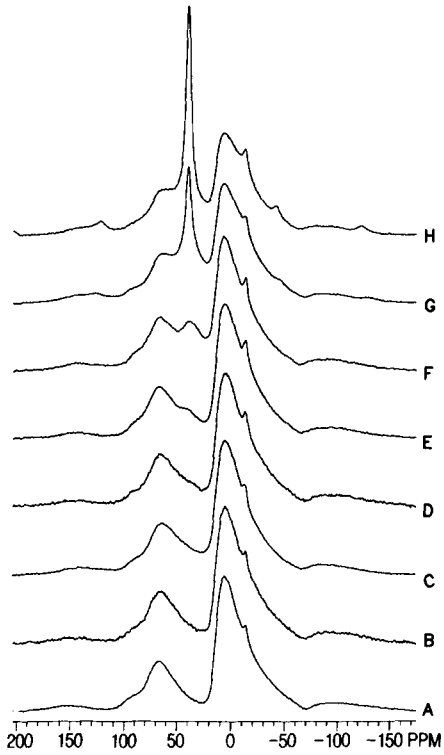

FIG. 11. ^{27}Al BD/MAS NMR spectra of calcined P-Mo(12)/Al_2O_3: (A), 0.0 wt% P; (B), 0.5 wt% P; (C), 1.0 wt% P; (D), 2.0 wt% P; (E), 4.0 wt% P; (F), 6.0 wt% P; (G), 10.0 wt% P; (H), 12.0 wt% P.

P–Ni–Mo/Al_2O_3

The phenomena found in the P/Al_2O_3, P–Ni/Al_2O_3, and P–Mo/Al_2O_3 samples can be used to explain the FT-IR spectra of CO adsorbed onto reduced P–Ni–Mo/Al_2O_3 (Fig. 13). CO adsorbed on reduced Ni(4)–Mo(8)/Al_2O_3 produces signals at 1950, 2065, and 2170 cm^{-1} (Fig. 13(c)), and these can be assigned to bridging CO on Ni^0, linear CO on Ni^0 and a combination of CO on Mo^{5+} and Mo^{4+}. This spectrum can be compared to CO adsorbed onto Ni(4)/Al_2O_3 and Mo(8)/Al_2O_3 (Figs. 13(a) and (b)). The addition of 4 wt% Ni to Mo(8)/Al_2O_3 results in a decrease in the densities of both the Mo and Ni adsorbing sites due to the formation

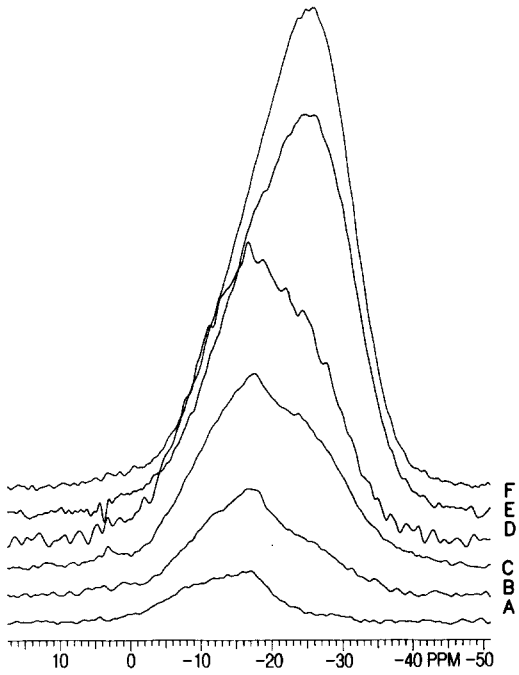

FIG. 12. ^{31}P BD/MAS NMR spectra of calcined P-Mo(8)/Al_2O_3: (A), 0.5 wt% P; (B), 1.0 wt% P; (C), 2.0 wt% P; (D), 3.0 wt% P; (E), 4.0 wt% P; (F), 6.0 wt% P.

of nickel molybdate (*47*). Molybdenum has also been shown to disperse the nickel on the catalyst surface (*48*). The addition of 0.5 wt% P to Ni(4)–Mo(8)/Al_2O_3 causes an increase in the intensity of all the bands. Previous studies have shown that nickel interacts with octahedral molydenum to form a new Ni–Mo species which is catalytically active (*49, 50*). We have shown earlier that phosphorus alters the molybdenum oxide structure on the alumina surface, resulting in a greater density of octahedral molybdate species relative to tetrahedral MoO_4^{2-}. We suggest that since phosphorus promotes the formation of the octahedral molybdate species in the P–Mo/Al_2O_3 samples, it may also promote the formation of the catalytically active Ni–Mo species in the P–Ni–Mo/Al_2O_3 samples. This Ni–Mo species would therefore be the precursor to the Ni–Mo–S site in the sulfided catalyst.

However, increasing the phosphorus up to 1.0 wt% causes a decrease in the density of the Ni^0 band, due to the formation of nickel phosphate. The addition of 2 wt% P causes the band at 2177 cm^{-1} to decrease,

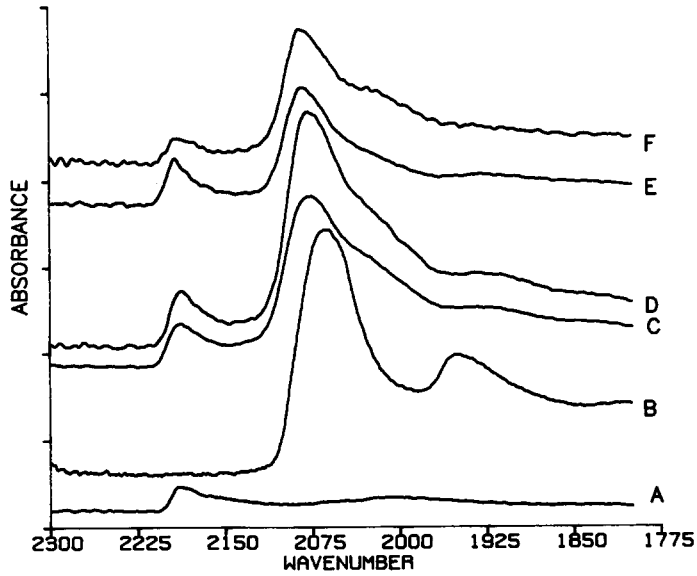

FIG. 13. IR spectra of CO adsorbed on reduced samples: (A), Mo(8)/Al_2O_3; (B), Ni(4)/Al_2O_3; (C), Ni(4)–Mo(8)/Al_2O_3; (D), P(0.5)–Ni(4)–Mo(8)/Al_2O_3; (E), P(1)–Ni(4)–Mo(8)/Al_2O_3; (F), P(2)–Ni(4)–Mo(8)/Al_2O_3.

revealing that the concentration of surface Mo^{5+} and Mo^{4+} has decreased. There is a further decrease in the density of Ni^0 as evidenced by the loss in intensity of the 2065 cm^{-1} band. These changes are due to the formation of either nickel molybdate or nickel phosphate.

CONCLUSION

We have shown that the combination of FT-IR, XRD and ^{31}P and ^{27}Al MAS NMR experiments is a very powerful tool for elucidating the surface structures of phosphorus containing catalysts. From this work we can make several conclusions concerning the effect of phosphorus on the surface structure of Ni–Mo/Al_2O_3 hydrotreating catalysts in the calcined and reduced state. We can also use these results to suggest explanations for the observed trend in HDN and HDS activities of the sulfided P–Ni–Mo/Al_2O_3 catalysts as a function of phosphorus loading (*13*).

The important conclusions from this work are as follows:

1. Phosphoric acid reacts with the alumina hydroxyls to produce monomeric and polymeric phosphate species, and at high phosphorus loading amorphous and crystalline aluminum phosphates are formed.

2. Ni^{2+} reacts with the phosphate anions during calcination to produce nickel phosphate.

3. The presence of up to 1.5 wt. % P in molybdenum containing catalysts promotes the formation of octahedral molybdates; we suggest that this species is the precursor to the stacking Ni–Mo–S species which has been shown to be the active site for the HDN and HDS reactions. Above 2 wt. % P, phosphorus promotes the formation of MoO_3 and $Al_2(MoO_4)_3$ in Mo/Al_2O_3 samples.

4. The addition of 0.5 wt. % P to Ni(4)–Mo(8)/Al_2O_3 causes an increase in the density of CO adsorbing sites; this can be attributed to an increase in a Ni–Mo interaction which is the result of the change in molybdate structure brought about by the phosphorus. Increasing the phosphorus loading further causes a decrease in the density of adsorbing sites, possibly due to the formation of either nickel phosphate or nickel molybdate.

REFERENCES

1. Mahanty, S., Saraf, D. N., and Kunzru, D., *Erdoel Kohle, Erdgas, Petrochem.* **43**(9), 359 (1990).
2. Hohnholt, J. F., and Fausto, C. Y., *Chem. Eng. Prog.* **81**(6), 47 (1985).
3. Morales, A., Ramirez de Agudelo, M. M., and Hernandez, F., *Appl. Catal.* **41,** 261 (1988).
4. Lopez Cordero, R., Gil Llambias, F. J., Palacios, J. M., Fierro, J. L. G., and Lopez Agudo, A., *Appl. Catal.* **56,** 197 (1989).
5. Gishti, K., Iannibello, A., Marengo, S., Morelli, G., and Tittarelli, P., *Appl. Catal.* **12,** 381 (1984).
6. Lopez Cordero, R., Esquivel, N., Lazaro, J., Fierro, J. L. G., and Lopez Agudo, A., *Appl. Catal.* **48,** 341 (1989).
7. Stanislaus, A., Absi-Halabi, M., and Al-Dolama, K., *Appl. Catal.* **39,** 239 (1988).
8. Atanasova, P., Halachev, T., Uchytil, J., and Kraus, M., *Appl. Catal.* **38,** 235 (1988).
9. Lopez Cordero, R., Lopez Guerra, S., Fierro, J. L. G., and Lopez Agudo, A., *J. Catal.* **126,** 8 (1990).
10. Sajkowski, D. J., Miller, J. T., Zajac, G. W., Morrison, T. I., Chen, H., and Fazzini, D. R., *Appl. Catal.* **62,** 205 (1990).
11. Spojakina, A., Damyanova, S., Petrov, L., and Vit, Z., *Appl. Catal.* **56,** 163 (1989).
12. Mangnus, P. J., van Veen, J. A. R., Eijsbouts, S., De Beer, V. H. J., and Moulign, J. A., *Appl. Catal.* **61,** 99 (1990).
13. D. Chadwick, D. W., Aitchison, R., Badilla-Ohlbaum, R., and Josefsson, L., *in* "Preparation of Catalysts III" (G. Poncelet *et al.*, Eds.), Vol. 16, p. 223. Elsevier, Amsterdam, 1983.
14. Fitz, C. W., and Rase, H. F., *Ind. Eng. Chem. Prod. Res. Dev.* **22,** 40 (1983).
15. Tischer, R. E., Narain, N. R., Stiegel, G. J., and Cillo, D. L., *Ind. Eng. Chem. Prod. Res. Rev.* **26,** 422 (1987).
16. Hopkins, P. D., and Meyers, B. L., *Ind. Eng. Chem. Prod. Res. Dev.* **22,** 421 (1983).
17. Ramirez de Agudelo, M. M., and Morales A., *in* "Proceedings, 9th International Congress on Catalysis, Calgary, 1988" (M. J. Phillips and M. Ternan, Eds.), Vol. I, p. 128. The Chemical Institute of Canada, Ottawa, 1988.
18. Knozinger, H., and Ratnasamy, P., *Catal. Rev. Sci. Eng.* **71**(1), 31 (1978).
19. Peri, J. B., *J. Phys. Chem.* **69,** 211 (1965).
20. van Veen, J. A. R., Hendriks, P. A. J. M., Romers, E. J. G. M., and Andrea, R. R., *J. Phys. Chem.* **94,** 5282 (1991).

21. Peri, J. B., *Discuss. Faraday Soc.* **52,** 55 (1971).
22. Segawa, K., and Hall, W. K., *J. Catal.* **77,** 221 (1982).
23. O'Young, C, Yang, C., DeCanio, S. J., Patel, M. S., and Storm, D. A., *J. Catal.* **113,** 307 (1988).
24. van Wazer, J. R., Callis, C. F., and Shoolery, J. N., *J. Chem. Soc.* **74,** 4945 (1955).
25. Callis, C. F., Van Wazer, J. R., Shoolery, J. N., and Anderson, W. A., *J. Chem. Soc.* **79,** 2722 (1957).
26. Uhlmann, D., Roske, I., Hupfer, M., and Ohms, G., *Wat. Rev.* **24,** 1355 (1990).
27. Tapp, N. J., Milestone, N. B., Bowden, M. E., and Meinhold, R. H., *Zeolites* **10,** 105 (1990).
28. Jahn, E., Muller, D., and Becker, K., *Zeolites* **10,** 151 (1990).
29. Morris, H. D., and Ellis, P. D., *JACS* **111,** 6045 (1989).
30. Galuszka, J., and Amenomiya, Y., *in* "Catalysis on the Energy Scene" (S. Kaliaguine and A. Mahay, Eds.), p. 63. Elsevier Science Publishers B. V., Amsterdam, 1984.
31. Little, L. H., "Infrared Spectra of Adsorbed Species." Academic Press, New York, 1966.
32. Hair, M. L., "Infrared Spectroscopy in Surface Chemistry." Marcel Dekker, New York, 1967.
33. Morales, A., and Ramirez de Agudelo, M. M., *Appl. Catal.* **23,** 23 (1986).
34. Dufresne, P., Payen, E., Grimblot, J., and Bonnelle, J. P., *J. Phys. Chem.* **85,** 2344 (1981).
35. Eijsbouts, Van Gruijthuijsen, L., Volmer, J., De Beer, V. H. J., and Prins, R., *in* "Advances in Hydrotreating Catalysts" (Occelli, M. L., and R. G. Anthony, Eds.), p. 79. Elsevier Science Publishers B. V., Amsterdam, 1989.
36. Mangnus, P. J., de Beer, V. H. J., and Moulijn, J. A., *Appl. Catal.* **67,** 119 (1990).
37. DeCanio, E. C., and Storm, D. A., *J. Catal.* **130,** 657 (1991).
38. Millman, W. S., Crespin, M., Cirillo, A. C., Jr., Abdo, S., and Hall, W. K., *J. Catal.* **60,** 404 (1979).
39. Peri, J. B., *J. Phys. Chem.* **86,** 1615 (1982).
40. Delgado, E., Fuentes, G. A., Hermann, C., Kunzmann, G., and Knozinger, H., *Bull. Soc. Chim. Belg.* **93,** 735 (1984).
41. Zaki, M. I., Vielhaber, B., and Knozinger, H., *J. Phys. Chem.* **90,** 3176 (1986).
42. Zingg, D. S., Makovsky, L. E., Tischer, R. E., Brown, F. R., and Hercules, D. M., *J. Phys. Chem.* **84,** 2898 (1980).
43. Hall, W. K., *in* "Proceedings, 4th International Conference on the Chemistry and Uses of Molybdenum," p. 224. Climax Molybdenum Co., Ann Arbor, Mich., 1982.
44. Jeziorowski, H., and Knozinger, H., *J. Phys. Chem.* **83,** 1166 (1979).
45. van Veen, J. A. R., De Wit, H., Emeis, C. A., and Hendriks, P. A., *J. Catal.* **107,** 579 (1987).
46. McMillan, M., Brinen, J. S., and Haller, G. L., *J. Catal.* **97,** 243 (1986).
47. Stencel, J. M., Makovsky, L. E., Diehl, J. R., and Sarkus, T. A., *J. Catal.* **95,** 414 (1985).
48. Jeziorowski, H., Knozinger, H., Taglauer, E., and Vogdt, C., *J. Catal.* **80,** 286 (1983).
49. Kasztelan, S., Grimblot, J., and Bonnelle, J. P., *J. Phys. Chem.* **91,** 1503 (1987).
50. Topsoe, N.-Y., and Topsoe, H., *J. Catal.* **84,** 386 (1984).